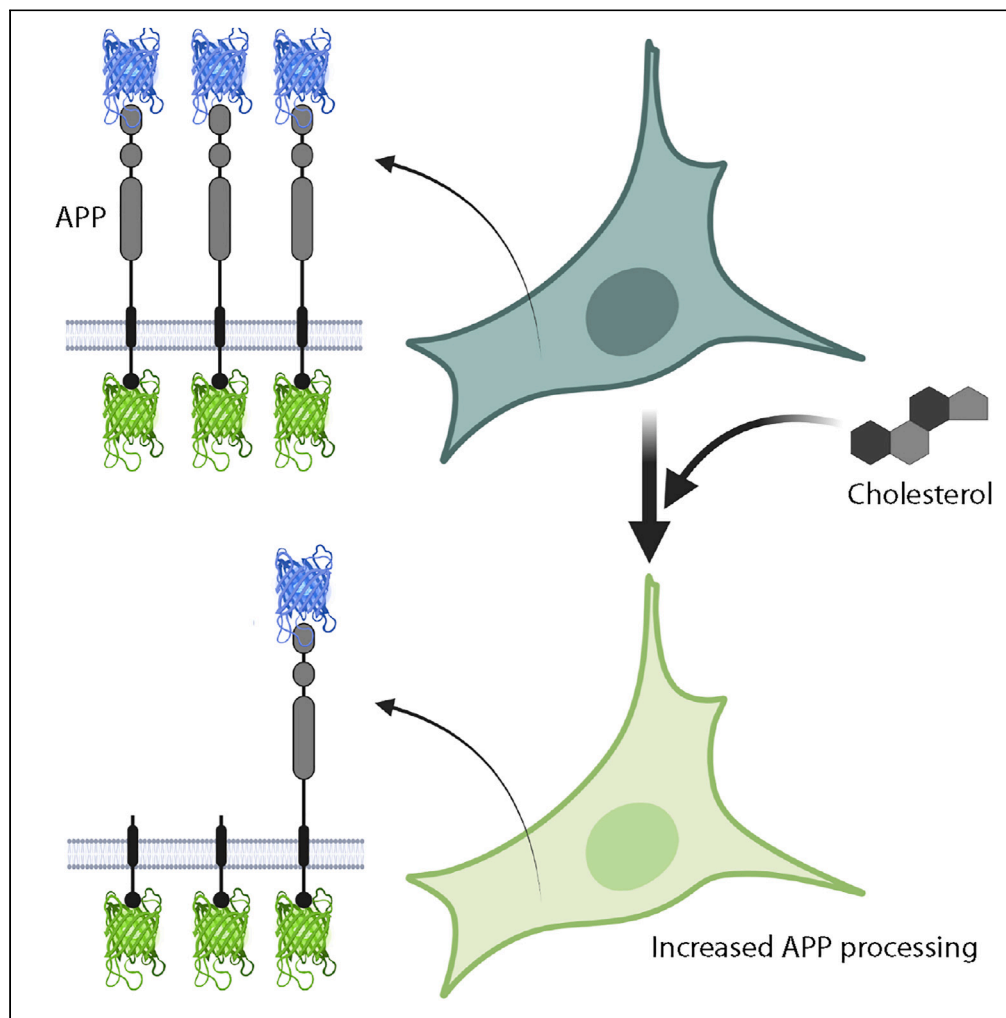# iScience

Article

APP and Bace1: Differential effect of cholesterol enrichment on processing and plasma membrane mobility

Claudia Capitini,
Alessandra Bigi,
Niccolò Parenti, ...,
Francesco
Annunziato,
Francesco Saverio
Pavone, Martino
Calamai

calamai@lens.unifi.it

Highlights

Cholesterol enrichment proportionally increases the cleavage of APP by Bace1

Bace1 is significantly more mobile than APP on the plasma membrane

No evidence for APP or Bace1 re-localization in rafts after cholesterol enrichment

Article

APP and Bace1: Differential effect of cholesterol enrichment on processing and plasma membrane mobility

Claudia Capitini,[1,2] Alessandra Bigi,[3] Niccolò Parenti,[2] Marco Emanuele,[2] Niccolò Bianchi,[2] Roberta Cascella,[3] Cristina Cecchi,[3] Laura Maggi,[4] Francesco Annunziato,[4] Francesco Saverio Pavone,[1,2,5] and Martino Calamai[2,5,6,*]

SUMMARY

High cholesterol levels are a risk factor for the development of Alzheimer's disease. Experiments investigating the influence of cholesterol on the proteolytic processing of the amyloid precursor protein (APP) by the β-secretase Bace1 and on their proximity in cells have led to conflicting results. By using a fluorescence bioassay coupled with flow cytometry we found a direct correlation between the increase in membrane cholesterol amount and the degree of APP shedding in living human neuroblastoma cells. Analogue results were obtained for cells overexpressing an APP mutant that cannot be processed by α-secretase, highlighting the major influence of cholesterol enrichment on the cleavage of APP carried out by Bace1. By contrast, the cholesterol content was not correlated with changes in membrane dynamics of APP and Bace1 analyzed with single molecule tracking, indicating that the effect of cholesterol enrichment on APP processing by Bace1 is uncoupled from changes in their lateral diffusion.

INTRODUCTION

The accumulation of the amyloid-β peptide (Aβ) as misfolded extracellular amyloid fibrils represents one of the main hallmarks of Alzheimer's disease (AD) pathology.[1] The pathogenic Aβ peptide generates from the sequential proteolytic cleavage of the amyloid precursor protein (APP) by the β-secretase Bace1 and the γ-secretase complex.[2–4] Specifically, the cleavage performed by Bace1 determines the release of the soluble APP β fragment (sAPPβ), whereas the remaining C-terminal fragment (CTF) can be processed by γ-secretase, causing the release of Aβ. Alternatively, and in most cases, APP is cleaved by the α-secretase ADAM10, with the consequent release of the soluble and non-amyloidogenic APP α fragment (sAPPα).

Many efforts have been made to identify the factors driving the activity of the secretases responsible for the cleavage of APP. Cholesterol is particularly significant in the context of AD,[5–8] especially considering the genetic link between the risk of developing AD and the ε4 allele of apolipoprotein E, a protein that regulates the cholesterol homeostasis.[9] It has been proved that changes in cholesterol levels can affect APP metabolism,[7,10–12] however most of the experiments evaluated the consequences of cholesterol depletion. Fewer studies have focused on the direct effects of cholesterol enrichment. Cholesterol increase was found to be followed by an increase in sAPPβ and Aβ secretion, whereas decreasing sAPPα,[13,14] and by the up-regulation of the proteolytic activity of Bace1.[15] However, another study found that the increase in Bace1 activity was not statistically significant following cholesterol enrichment.[16] It was also reported that a greater Aβ production in the presence of increased cholesterol levels was associated with higher expression levels of Bace1 in mice.[17] Higher cholesterol levels were shown to increase the endocytosis of APP,[18] possibly through dynein mediation.[16] Two independent groups studied the changes in proximity of Bace1 and APP stimulated by cholesterol, obtaining opposite results using the same advanced microscopy approach based on Total Internal Reflection Fluorescence (TIRF), Fluorescence Lifetime Imaging (FLIM) and Fluorescence Resonance Energy Transfer (FRET). In particular, one group found that higher cholesterol promotes a selective increase in proximity of Bace1 and APP on the cell surface and not intracellularly,[16] whereas the other found Bace1 and APP are in close proximity only within the cell, displaying reduced intracellular proximity when increasing cholesterol, or in cells from patients affected by Neimann-Pick type C

[1]Dipartimento di Fisica e Astronomia, Università degli Studi di Firenze, 50019 Florence, Italy

[2]European Laboratory for Non-linear Spectroscopy (LENS), University of Florence, 50019Florence, Italy

[3]Department of Experimental and Clinical Biomedical Sciences, University of Florence, 50134 Florence, Italy

[4]Department of Experimental and Clinical Medicine, University of Florence 50134 Florence, Italy

[5]National Institute of Optics, National Research Council of Italy (CNR), Largo Fermi 6, 50125Florence, Italy

[6]Lead contact

*Correspondence:
calamai@lens.unifi.it

https://doi.org/10.1016/j.isci.2023.106611

Table 1. Effective cholesterol concentrations in relation to β-CD-chol amounts*

β-CD-chol	Cholesterol
0.2 mg/mL	8 μg/mL (∼20 μM)
0.4 mg/mL	16 μg/mL (∼40 μM)
0.6 mg/mL	24 μg/mL (∼60 μM)
0.8 mg/mL	32 μg/mL (∼80 μM)
1.0 mg/mL	40 μg/mL (∼100 μM)

*As indicated for the product Cholesterol-Water Soluble C4951 (Sigma-Merck).

(in which cholesterol is pathologically accumulated), and did not find any concomitant change in proximity of Bace1-APP on the plasma membrane.[13,19] Other studies suggest that high levels of cholesterol could promote the redistribution of APP on the cell membrane, inducing its translocation into membrane-rafts, cholesterol-enriched microdomains of the plasma membrane putatively containing Bace1 and the Presenilin-1 (PS1) complex, the enzymes responsible for cleaving APP into Aβ peptide.[11,15,20,21] Rafts have been commonly defined on a biochemical basis using harsh conditions (detergent resistant membranes-DRM- isolation)[22] but are rather difficult entities to be classified[23] and might not be the direct reflection of the same protein localization in the plasma membrane.[24]

Here, we have further contributed to elucidate the role of membrane cholesterol on APP processing by Bace1, whereas evaluating any effect on Bace1 and APP dynamics on the plasma membrane. We chose to investigate only the enrichment in cholesterol, as methyl-β-cyclodextrin and statins can induce other alterations in addition to inducing cholesterol depletion.[25–27] To date, commercial fluorometric assay kits (e.g., Sigma-Aldrich, Abcam) are available to measure the enzymatic activity of the secretases. However, although characterized by high sensitivity and stability, they can only be applied to samples purified from cell lysates. Recently, we developed a rapid bioassay capable of gaining visible and quantitative information on the proteolytic processing of APP directly in living cells.[28] This system involves the use of a chimeric construct of APP695 (the major isoform of APP expressed in the brain[29]) with two different fluorescent proteins fused at the N-terminal (extracellular) and C-terminal (intracellular) ends. The intensity ratio of the two fluorescent proteins, determined by means of microscopy or flow cytometry, can be used to monitor changes occurring in the proteolytic processing of APP.[28,30,31] We demonstrated that this probe can be cleaved by Bace1 and ADAM10, and it was successfully used in several types of cellular models, including human neuroblastoma cells and rodent hippocampal neurons.[28,31]

In addition, in the attempt to test the raft translocation hypothesis and investigate APP and Bace1 proximity on the cell surface with an alternative method, we used single molecule tracking (SMT) experiments to investigate the dynamics of APP and Bace1 on the plasma membrane of human neuroblastoma cells both in basal conditions and on addition of increasing concentrations of cholesterol.

Our results strongly support a direct or indirect influence of cholesterol on the initial proteolytic cleavage of APP, with the processing rate increasing with the increase in membrane of cholesterol amount. On the other hand, we found that the lateral diffusion of APP and Bace1 can be influenced by cholesterol but in a manner not necessarily and uniformly correlated with the different cholesterol concentrations.

RESULTS

Cholesterol enrichment can decrease the metabolic activity of SH-SY5Y cells, but does not induce lipid peroxidation or apoptosis

SH-SY5Y neuroblastoma cells were incubated for 3 h with increasing concentrations of water soluble cholesterol (cholesterol-methyl-β-cyclodextrin, β-CD-chol) ranging from 0.2 to 1.0 mg/mL. Notably, the effective concentration of cholesterol is ∼25-folds lower than that of β-CD-chol (Table 1), and thus well within the concentration of free cholesterol found in human interstitial fluid (∼10 μg/mL).[32] The Amplex Red assay indicated that the membrane cholesterol content increased significantly already at 0.2 mg/mL β-CD-chol (137.78 ± 12.14 ng chol/μg protein) compared to basal cells (83.71 ± 11.61 ng chol/μg protein), reaching the maximum at 1.0 mg/mL β-CD-chol (241.54 ± 24.84 ng chol/μg protein) (Figure 1A). These results were further supported by confocal microscopy imaging using the fluorescent probe filipin III,[33] whose fluorescence intensity increased proportionally to β-CD-chol concentrations (Figure 1B).
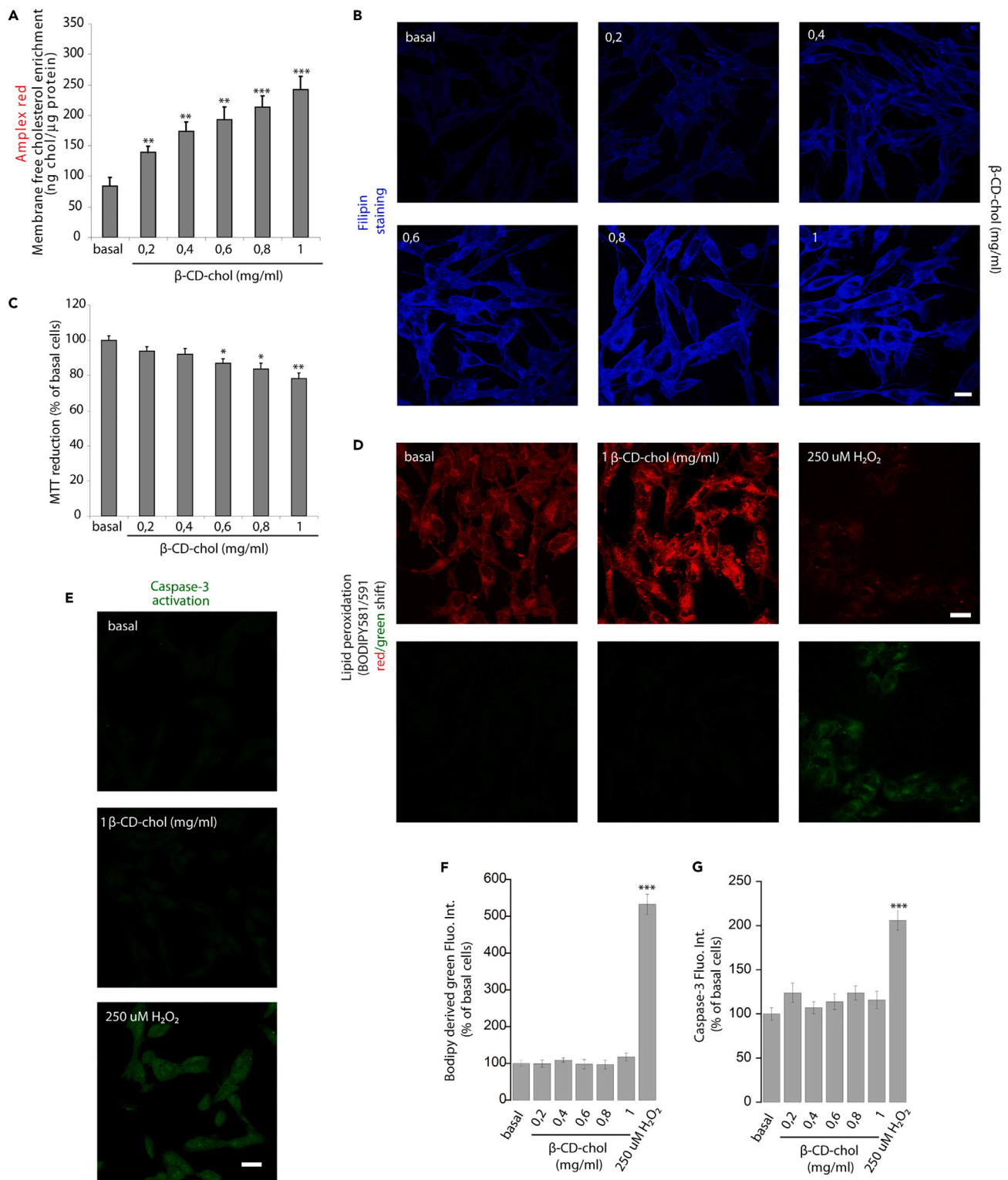
Figure 1. Effects of cholesterol enrichment on cellular viability

SH-SY5Y neuroblastoma cells were analyzed in basal conditions and after 3 h of incubation at different concentrations of β-CD-chol.

(A) Effective membrane cholesterol enrichment was quantified with the Amplex Red kit, as reported in the Methods section.

(B) Representative confocal microscope images of β-CD-chol content in SH-SY5Y cells probed with the fluorescent dye filipin III.

Figure 1. Continued

(C–G) Assessment of the toxic effects on SH-SY5Y cells exposed to increasing concentrations of cholesterol with MTT reduction assay (C), lipid peroxidation (D and F) and caspase-3 activation (E–G), together with representative confocal microscope images (D and E). Lipid peroxidation was investigated on the incubation with the fluorescent probe BODIPY 581/591 C11. Caspase-3 activity was assessed by using the FLICA reagent FAM-DEVD-FMK. 250 μM H_2O_2 was also tested as a control. Error bars correspond to standard errors of the means of n > 3 independent experiments. Student's t test for two distributions comparison. Single, double, and triple asterisks refer to $p < 0.05$, <0.01, and <0.001, respectively, with respect to basal conditions.

Potential side effects of the increase in cholesterol content on the metabolic activity of SH-SY5Y cells were monitored by the 3-(4,5-dimethylthiazol-2-yl)-2, 5-diphenyltetrazolium bromide (MTT) reduction inhibition assay, a widely used indicator of the rate of glycolytic NAD(P)H production. We found that the MTT reduction was progressively inhibited, with a decrease of approximately 20% at 1.0 mg/mL β-CD-chol (Figure 1C).

We then investigated whether the increment in membrane cholesterol content led to an increase in membrane lipid peroxidation, by using the fluorescent probe BODIPY 581/591 C11, which shifts its fluorescence from red to green in the presence of oxidizing agents. We found that the green fluorescence signals observed in membrane cholesterol-enriched cells did not differ from their respective in basal cells (Figures 1D–1F), indicating the absence of significant lipid peroxidation. On the contrary, cells treated with 250 μM H_2O_2 for 3 h showed a significant shift to green, indicating a high lipid peroxidation level.

We also evaluated whether an increased content of membrane cholesterol could lead to caspase-3 activation, an important marker of apoptotic cell death, by measuring the fluorescence of FLICA reagent FAM-DEVD-FMK covalently coupled to the active enzyme in living cells. Under our experimental conditions, the membrane cholesterol enrichment did not induce significant caspase-3 activation (Figures 1E–1G). By contrast, a significant activation of apoptotic cell death was observed on treatment with 250 μM H_2O_2 for 3 h.

Overall, we demonstrated that our treatment with soluble cholesterol results in higher cholesterol content in the plasma membrane and partially decreases the metabolic activity of SH-SY5Y cells, without however inducing lipid peroxidation and apoptosis.

Alterations in cellular cholesterol content drive proportional changes in mBFP-APP-mGFP processing

We investigated the effect of cholesterol on the proteolytic processing of APP by means of a previously developed flow cytometry bioassay which requires the use of an engineered construct containing the sequence of the APP695 isoform fused with two distinct fluorescent proteins located at the two extremities.[28] In the present study, for increasing compatibility with most common flow cytometry laser setups equipped with violet, blue and red lasers, we replaced the monomeric variant of the red fluorescent protein (mCherry, excitable with yellow laser) at the N-terminal (extracellular side) with the monomeric variant of the blue fluorescent protein (mBFP, excitable with the violet laser), keeping the monomeric variant of the green fluorescent protein (mGFP, excitable with the blue laser) at the C-terminal (intracellular side) (Figure 2A). The final construct was named mBFP-APP-mGFP. Changes in the cleavage rate of the N-terminal domain of APP are eventually translated in changes in the fluorescence intensity ratio between the blue and green signals. Similarly, we produced the fusion construct of the mutated form APP[P1] (mBFP-APP[P1]-mGFP), that can be cleaved almost exclusively by Bace1, owing to the Lys to Val substitution at position 612 that prevents α-secretase activity.[28,31,34]

SH-SY5Y neuroblastoma cells overexpressing mBFP-APP-mGFP were analyzed with flow cytometry 48 h after transfection. After Forward Scatter-Area/Side Scatter-Area (FSC-A/SSC-A) gating for discriminating live cells from cellular debris, an additional gating was applied to measure only the blue and green fluorescence intensity of the transfected cells (Figure 2B). The blue signal can originate from the full length chimeric construct (mBFP-APP-mGFP) and in part from the intracellular soluble fragments (mBFP-sAPPs) not yet released. On the other hand, the full length chimeric construct, the C-terminal fragments (CTFs-mGFP) and the APP intracellular domain (AICD-mGFP) account for the green signal.

The green fluorescence was found to significantly increase after 3h incubation of SH-SY5Y cells overexpressing mBFP-APP-mGFP or mBFP-APP[P1]-mGFP with increasing cholesterol concentrations (max ~10% increase at 1.0 mg/mL β-CD-chol). This indicates that the higher cholesterol content can somehow increase the synthesis of mBFP-APP-mGFP (or mBFP-APP[P1]-mGFP), or inhibit its degradation. By contrast, a similar proportional trend was not observed for the blue fluorescence, suggesting changes in the processing rate of mBFP-APP-mGFP (or mBFP-APP[P1]-mGFP) (Figure 2C). As it could be expected given the weak
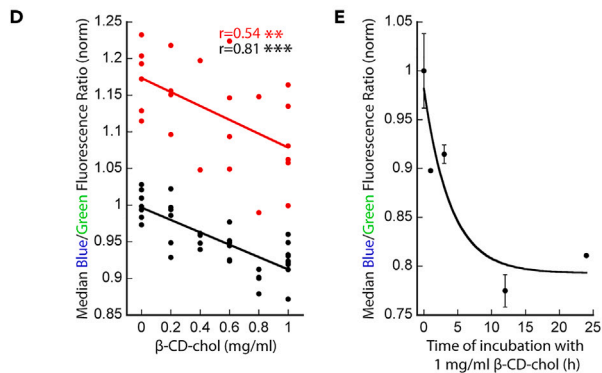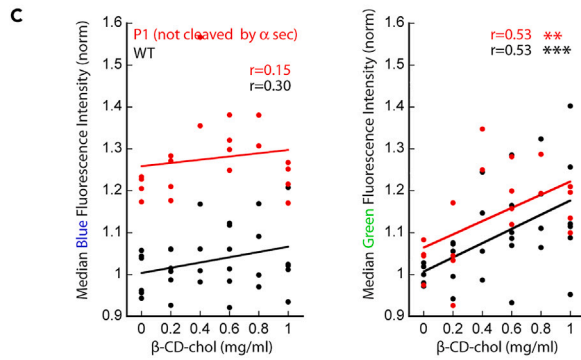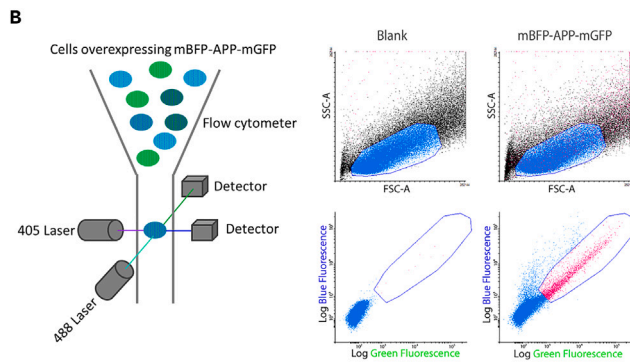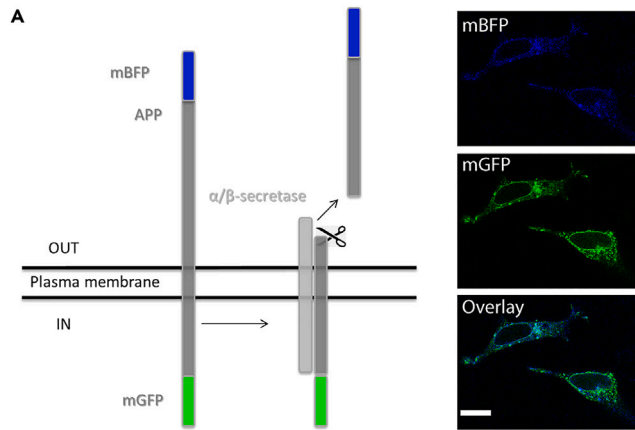
Figure 2. Increased processing of mBFP-APP-mGFP following cholesterol enrichment probed with flow cytometry

(A) Schematic representation of the bioassay rationale: changes in mBFP-APP-mGFP shedding rates are translated in changes in the ratio between the blue and green fluorescence intensity. Representative Maximum intensity projections of confocal z-stacks of living human SH-SY5Y cells overexpressing mBFP-APP-mGFP.

(B) Flow cytometry analysis of control cells and cells transfected with mBFP-APP-mGFP. Gating was applied for removing cell debris and selecting only the green and blue fluorescence of transfected cells.

(C and D) SH-SY5Y cells overexpressing mBFP-APP-mGFP (WT, black) or the mBFP-APPP1-mGFP mutant (P1, red) were incubated for 3 h at different β-CD-chol concentrations. (C) Correlation between β-CD-chol concentration and the median blue (b) and green (g) fluorescence intensities, or (D) b/g values, normalized to basal conditions.

(E) SH-SY5Y cells overexpressing mBFP-APP-mGFP incubated for different times with 1.0 mg/mL β-CD-chol. Each dot represents the median fluorescence value of >2000 transfected cells analyzed. r, linear correlation coefficient value. Single, double, and triple asterisks refer to $p < 0.05$, <0.01, and <0.001. Error bars, S.D. $n \geq 3$ independent experiments.

α-secretase activity on the mutated APP protein, the median blue fluorescence intensity was higher for mBFP-APPP1-mGFP than mBFP-APP-mGFP.

We then looked at the blue/green fluorescence intensity ratio (b/g) per cell (Figure 2D). A significant negative linear correlation was found between the median b/g values and the cholesterol content, with approximately 10% reduction in b/g values found at 1.0 mg/mL β-CD-chol. A comparable decrease was also found using mCherry-APP-mGFP (Figure S1). Around 20% higher b/g was observed under basal condition for mBFP-APPP1-mGFP compared to mBFP-APP-mGFP, attributable to the very limited activity of α-secretase on the APP mutant (Figure 2D). Accordingly, the potent inhibition of ADAM10 α secretase activity with the selective GI 254023X inhibitor showed similar b/g increase compared to mBFP-APPP1-mGFP (Figure S2). Notably, mBFP-APPP1-mGFP and mBFP-APP-mGFP displayed similar slopes, indicating that alteration in cholesterol levels could mainly affect the kinetics of β secretase cleavage.

A time course analysis of the b/g of mBFP-APP-mGFP in cells exposed to 1 mg/mL β-CD-chol showed a maximum decrease of 20% at 24 h (Figure 2E).

These data show that an increase in cellular cholesterol content leads to a proportional moderate increase in APP processing by β-secretase.

Higher amounts of intracellular CTFs-mGFP and extracellular mBFP-sAPPβ/mBFP-sAPPα ratio are found at higher cholesterol levels

We then examined by western blotting analysis the lysates and the extracellular medium obtained from SH-SY5Y cells overexpressing mBFP-APP-mGFP untreated or incubated for 3 h with 0.2, 0.6 and 1.0 mg/mL β-CD-chol.

For the lysate analysis we used antibodies against the C-terminal domain of APP, or specific for the soluble APP products following α- or β-secretase cleavage, anti-sAPPα and anti-sAPPβ, respectively (Figures 3A and 3B). The housekeeping protein α-tubulin was used as loading control. Although a slight but not significant increase was found for full length mBFP-APP-mGFP (revealed with anti-C-term APP, expected Mw = 132 kDa) and for mBFP-sAPPα on increasing cholesterol concentration, a significant positive correlation was found for CTFs-mGFP (expected Mw = 36–38 kDa), with a max ∼20% increase at 1.0 mg/mL β-CD-chol (Figures 3A and 3B). Of interest, the amount of intracellular mBFP-sAPPβ (expected Mw = 92 kDa) appeared to significantly increase at 0.2 mg/mL β-CD-chol and to return to untreated values at higher cholesterol concentrations. The presence of basal sAPPα fragments (expected Mw = 98 kDa) in cell lysates is not surprising and has already been demonstrated in other studies.[35–38]

The extracellular medium from different samples was analyzed using anti-sAPPα and re-probed with anti-sAPPβ following antibody stripping, and the results were expressed as mBFP-sAPPβ/mBFP-sAPPα ratio (Figures 3C and 3D). A significant positive correlation was found between the ratio values and the amount of cholesterol, with an approximate 20% increase at 1.0 mg/mL β-CD-chol. These data are in agreement with the observation that 100 μM cholesterol increases sAPPβ and decreases sAPPα secretion.[13]

These results corroborate the data obtained with flow cytometry, suggesting that the observed increase in green fluorescence is in part effectively because of an increase in CTFs-mGFP at higher cholesterol
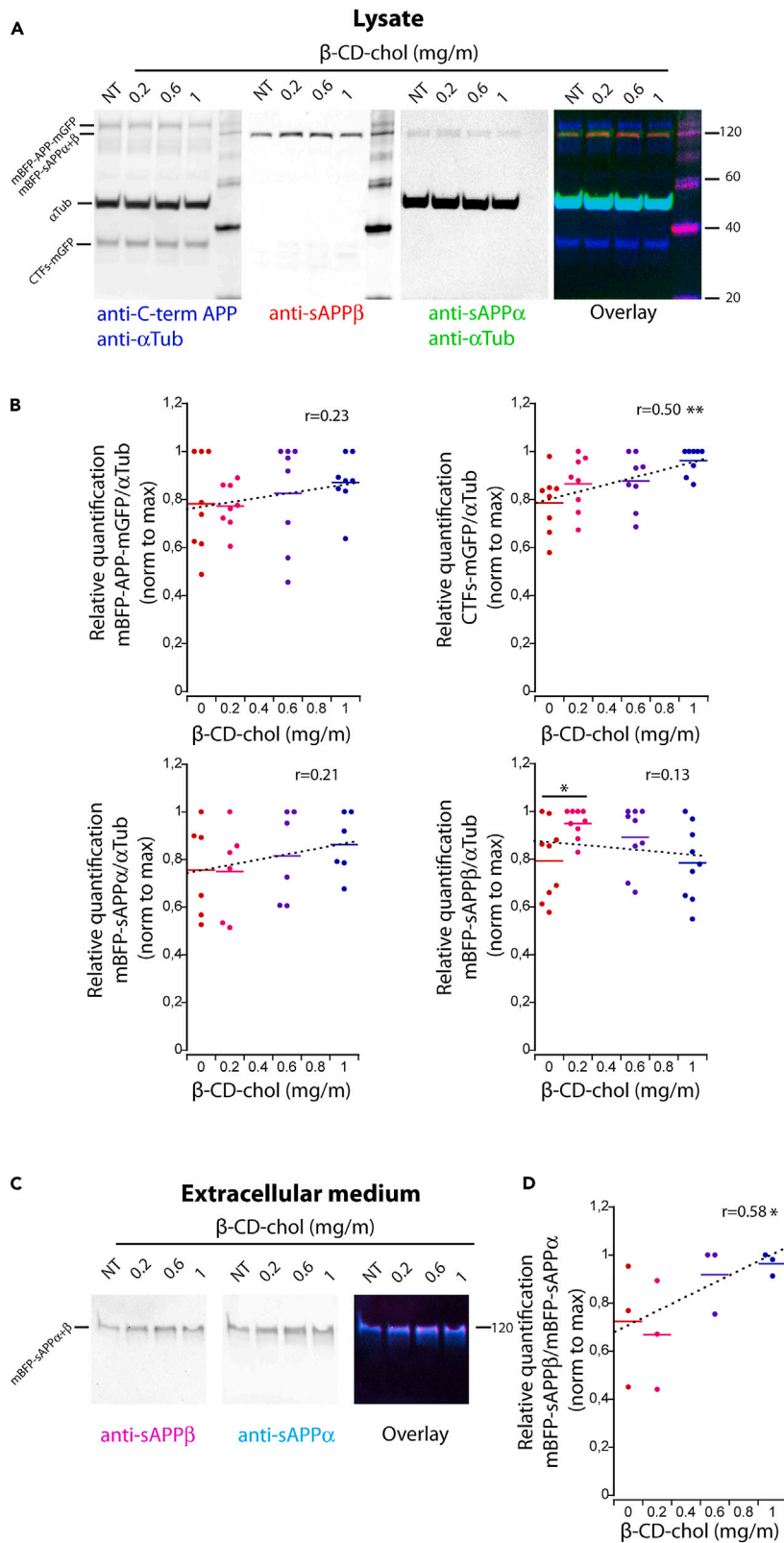
A

Lysate

β-CD-chol (mg/m)

anti-C-term APP
anti-αTub

anti-sAPPβ

anti-sAPPα
anti-αTub

Overlay

B

C

Extracellular medium

β-CD-chol (mg/m)

anti-sAPPβ   anti-sAPPα   Overlay

D

Figure 3. Analysis of changes in shedding products of mBFP-APP-mGFP following cholesterol enrichment

(A–D)SH-SY5Y cells overexpressing mBFP-APP-mGFP were incubated for 3 hat different β-CD-chol concentrations, and lysates (A and B) and extracellular medium (C and D) were subsequently collected and analyzed by Western blotting. (B and C) Representative lysate and medium blots repeatedly stripped and re-probed with primary antibodies against the C-terminal domain of APP, sAPPα, sAPPβ and α-tubulin. Each dot represents the signal intensity of the band first normalized to α-tubulin for lysates (B), or sAPPα for cell medium (D), and then normalized to the max value in each experiment. r, linear correlation coefficient value. Student's *t*test for two distributions comparison. Single, double, and triple asterisks refer to p < 0.05, <0.01, and <0.001. n ≥ 3 independent experiments.

concentrations, whereas the intracellular blue fluorescence does not increase proportionally as mBFP-sAPPβ is gradually released extracellularly.

APP and Bace1 plasma membrane dynamics and cholesterol display a non-monotonic relationship

To investigate if the cholesterol content could influence the membrane dynamics of APP and the β-secretase Bace1, we produced chimeric constructs of the two proteins, each one containing a monomeric variant of a fluorescent protein at the C-terminus (mGFP for APP and mBFP for Bace1) and the HA tag at the N-terminus, immediately after the SP (Figure 4A). We first ensured that the chimeric proteins were correctly targeted to the cell membrane by performing a surface immunolabeling of transfected human SH-SY5Y neuroblastoma cells (Figure 4B). Single HA-APP-mGFP or HA-Bace1-mBFP moving on the plasma membrane of living SH-SY5Y cells were then imaged with anti-HA primary antibodies and secondary antibodies coupled to QDs (Figure 4C, Videos S1, andS2). Trajectories of single HA-APP-mGFP or HA-Bace1-mBFP were extrapolated from the real time recordings and diffusion parameters were calculated. Surprisingly, HA-APP-mGFP mostly displayed a confined type of motion (with an average calculated confined area in which diffusion is restricted of 0.40 μm^2), as shown by the average MSD plot over time interval (Figure 4D). By contrast, the MSD plot for HA-Bace1-mBFP showed a rather linear relationship, indicating a more Brownian oriented type of motion. The measured instant diffusion coefficient (D) was found to be almost one order of magnitude lower for HA-APP-mGFP (median D = 0.020 μm^2 s^{-1}) than for HA-Bace1-mBFP (median D = 0.10 μm^2 s^{-1}) (Figure 4E). Also the percentage of spots classified as immobile (spots with D< 0.0001 μm^2 s^{-1}) was higher for HA-APP-mGFP (4%) than for HA-Bace1-mBFP (0.05%) (Figure 4F).

SH-SY5Y cells overexpressing HA-APP-mGFP or HA-Bace1-mBFP were then incubated for 3 h with increasing concentrations of β-CD-chol up to 1.0 mg/mL, and diffusion coefficients were measured (Figure 4G). In the case of HA-Bace1-mBFP the diffusion coefficient was significantly altered only at 0.8 mg/mL β-CD-chol, with a moderate decrease in median D of ∼30%. HA-APP-mGFP appeared to be more influenced by cholesterol levels, showing significant median D increases (∼70%) at 0.4, 0.8 and 1.0 mg/mL β-CD-chol and reduction at 0.2 mg/mL. Although a slight decrease in median diffusion was visible for HA-Bace1-mBFP at higher cholesterol concentrations, whereas the opposite effect was apparent for APP, the changes in median D of both proteins were not significantly linearly correlated (p>0.05) with the amount of supplemented β-CD-chol (Figure 4H).

These results show that Bace1 displays a higher mobility on the plasma membrane than APP, and that cholesterol can influence the diffusion of the two proteins, in particular APP, but following a non-monotonic relationship.

We tried to image association and cleavage of single APP molecules from Bace1, and if cholesterol could influence this. By using simultaneous dual color imaging of cells co-transfected with AP-APP and HA-Bace1-mBFP labeled, respectively, with streptavidin QD655 and primary anti-HA with secondary antibodies coupled to QD585, we were able to record only few events of interaction and co-diffusion of the two proteins under basal conditions (Figure S3). The limited number of events observable on the plasma membrane could be because of the fact that in our system the extracellular N-terminal of APP is labeled and therefore, if the cleavage (on which the fluorescent probe bound to APP is lost in the extracellular medium) occurs immediately after the interaction between APP and Bace1 takes place, association events might not be detectable. Or it could be simply be the consequence of limited proximity and interaction of APP and Bace1 on the cell surface.[13] We could see some Bace1 molecules, normally mobile, bound to confined APP (not the opposite), or changing type of motion, from Brownian to confined on interaction with APP (Figure S3B, Video S3). We also imaged few events of active intracellular transport in which single APP and Bace1 molecules were co-localizing (FigureS3C, Video S4). As the detected events remained rare
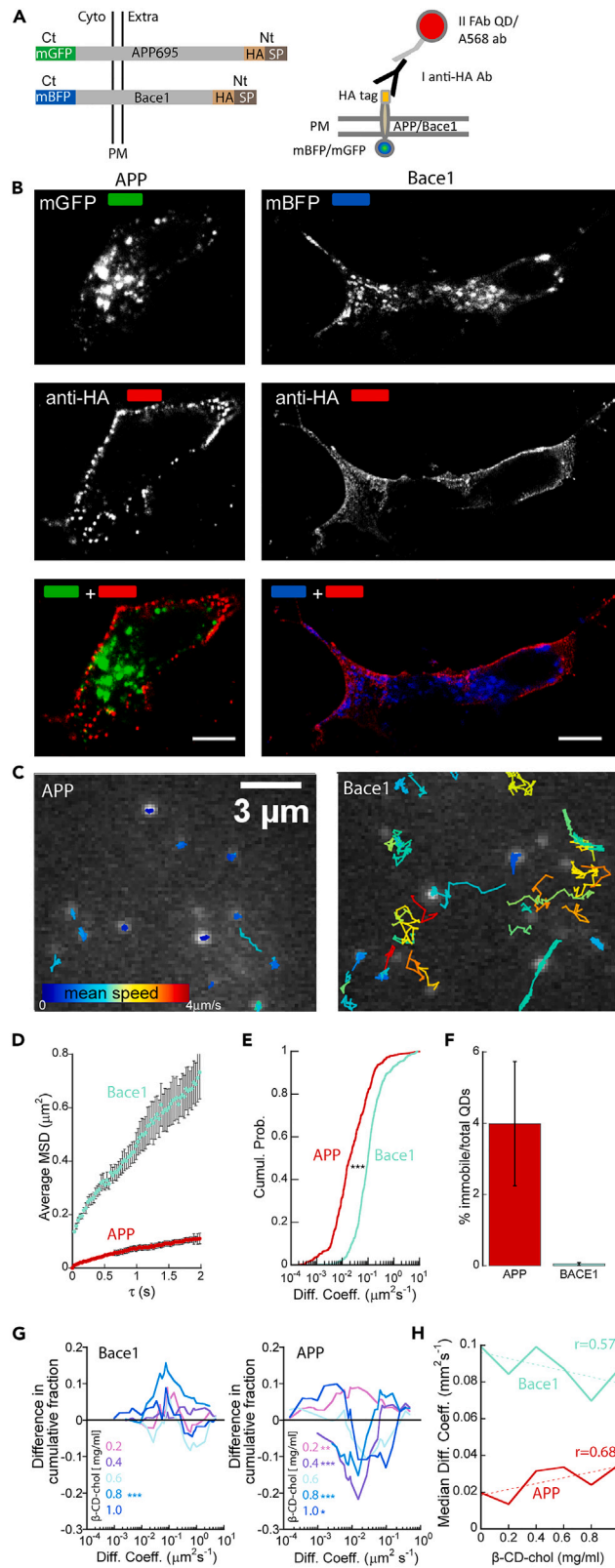
Figure 4. Dynamics of APP and Bace1 on the plasma membrane following cholesterol enrichment probed with single molecule tracking

(A–H) Lateral diffusion of (A) Design of the various chimeric constructs and labeling scheme. The N-terminal HA tag is inserted after the signal peptide (SP) for plasma membrane targeting. SH-SY5Y cells were transfected separately with the chimeric constructs HA-APP-mGFP and HA-Bace1-mBFP and labeled with primary anti-HA antibody and secondary antibody coupled to Alexa 568 (B) for confocal imaging, or to QDs 655 for single molecule tracking (C–H). The average mean square displacement (MSD) (D), diffusion coefficients (E, G, and H) and percentage of immobile spots were calculated from >100 trajectories from n > 3 experiments for each condition. (G) The differences in cumulative fraction of cells exposed for 3 h to different amounts of cholesterol were calculated with respect to the diffusion coefficient values of the basal condition of the two proteins (black line): positive values indicate a fraction of molecules with a certain diffusion coefficient larger than that observed for basal conditions, indicating an overall decreased mobility; conversely a trend of negative values point at an increased mobility. p values were calculated by Kolmogorov-Smirnov test, using the maximum difference in cumulative fraction between cells incubated with different cholesterol concentrations and basal as statistic. r, linear correlation coefficient value. Single, double, and triple asterisks refer to $p < 0.05$, <0.01, and <0.001. Error bars, S.D.

under cholesterol enriched conditions, it was not possible to assess any statistically significant change in the number or type of events.

DISCUSSION

The first set of experiments using mBFP-APP-mGFP was directed at probing any effect of cholesterol on APP shedding. If cholesterol enrichment was incrementing exclusively the processing rate of mBFP-APP-mGFP, we should had seen a decrease in the amount of full length protein, with higher CTFs-mGFP levels and higher extracellular mBFP-sAPPβ/mBFP-sAPPα values, in the western blots, and a decrease in the blue channel fluorescence intensity without variations in the green channel in FACS experiments (Figure 5A).

On the other hand, if cholesterol was influencing only the synthesis (or degradation) rate of mBFP-APP-mGFP, we would have seen a proportional increase in the blue and green fluorescence intensities in FACS, accompanied by similar increases in full length protein and CTFs-mGFP, without variations in mBFP-sAPPβ/mBFP-sAPPα values.

By contrast, our FACS experiments on the dependence of the processing rate of mBFP-APP-mGFP on cholesterol show a slight but significant increase in the green channel fluorescence intensity not followed by a similar trend in the blue channel at higher cholesterol concentrations (Figure 5A). In analogue western blots experiments we observed a moderate increase in the levels of intracellular CTFs-mGFP and of extracellular mBFP-sAPPβ relative to mBFP-sAPPα. The intracellular levels of mBFP-sAPPα and full length mBFP-APP-mGFP were not significantly altered, although a very modest increase seems present. Our experiments therefore demonstrate that cholesterol enrichment (1) is correlated with increased mBFP-APP-mGFP processing (2) can alter the cellular levels of mBFP-APP-mGFP (either increasing its synthesis or inhibiting its degradation) in our model system. Of interest, another group found an increase in intracellular levels of full length APP at higher β-CD-chol concentrations.[39] As our construct was under the CMV promoter, not the endogenous one, it is however possible that the lack of the expected decrease in full length mBFP-APP-mGFP levels is just a model artifact.

Analogue flow cytometry experiments carried out using mBFP-APP[P1]-mGFP (which cannot be cleaved by α-secretase), showing a data trend similar to mBFP-APP-mGFP, prove that at least the β-secretase processing is affected by cholesterol levels. In our system we cannot discriminate if mBFP-sAPPβ shedding takes place at the endosomal level and then is released extracellularly after endosomal recycling to the plasma membrane, or directly on the cell surface as proposed by other studies.[21,40,41] Notably, the increase in APP shedding activity observed in the present work at increasing cholesterol concentration is concomitant with a decrease in MTT reduction, which can be related to metabolic activity, without any major effect on cell viability.

We then investigated if alterations in the processing of APP because of cholesterol could be directly related to changes in the lateral diffusion of APP and Bace1 on the plasma membrane. Also in this case we limited our experiments to cholesterol loading in place of depletion, as effects on diffusion of rafts and membrane proteins were shown to strongly depend on the method of depletion.[42] The association of APP and Bace1 with membrane rafts is controversial.[43] According to a common hypothesis, Bace1 would localize mostly in membrane rafts, whereas APP would partition between raft and non-raft regions.[11,15,20] It was proposed that an enrichment in cholesterol could promote the proximity of APP
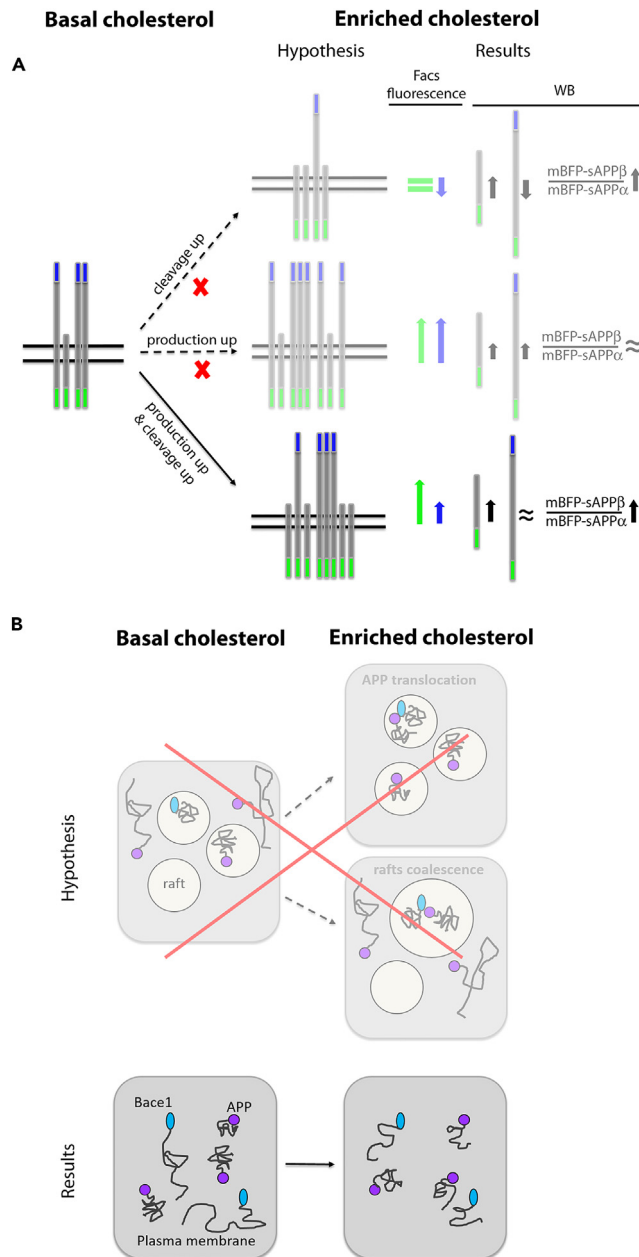
Figure 5. Schematic representation of the effect of cholesterol on APP processing and dynamics

(A) The increase in green fluorescence not followed by an equivalent increase in blue fluorescence observed with flow cytometry, together with increased intracellular C-term APP levels without parallel increase in full length APP, and increased extracellular sAPPβ amounts with respect to sAPPα, observed with western blotting, suggest a higher β-secretase processing of APP when cells are exposed to cholesterol enrichment conditions.

(B) Single molecule tracking data indicate that Bace1 has a higher mobility on the plasma membrane compared to APP, and that cholesterol enrichment has very limited effect on the mobility of Bace1, whereas affecting the mobility of APP in a manner not directly correlated with its content. Our data do not provide any evidence to support the hypothesis that cholesterol is a major factor governing APP and Bace1 partitioning into raft-like domains.

and Bace1, facilitating the cleavage, either through the translocation of APP in membrane rafts containing Bace1, or through the coalescence of rafts containing APP and Bace1. However, only a small fraction of APP and Bace1 was found associated with DRMs and the likelihood that APP and Bace1were in same rafts seemed low.[21]

Molecules located in raft microdomains should in general display lower diffusion rates compared to molecules located in more fluid and disordered part of the plasma membrane, and with our single molecule tracking experiments we could have been able to discriminate, in principle, changes in the dynamic partitioning between the raft and non-raft populations (if any).[24,42] If Bace1 was mostly localized in raft domains, a lower mobility would have been expected compared to that of APP. By contrast, we found (using the same tag and same probe for labeling) that the lateral diffusion of Bace1 was one order of magnitude higher than that of APP. The median diffusion coefficient found for our construct HA-Bace1-mBFP (median D = 0.10 µm^2 s^{-1}) is aligned with previous results on Bace1 surface dynamics obtained by other groups: D = 0.2–0.6 µm^2 s^{-1} using the probe siR-Bace1,[44] D = 0.47 µm^2 s^{-1} using the construct pHBace.[40] In the latter study, in agreement with our observations, the analogue construct pHAPP did not show any lateral diffusion on the plasma membrane. Moreover, the average D of glycosylphosphatidylinositol-anchored (GPI) GFP, a consensus raft markers, is 1–1.3 µm2/s,[45,46] very far from those observed for Bace1 and APP. These data indicate that the localization of these two proteins inside or outside ordered microdomains is not the prominent factor governing their diffusion on the plasma membrane. Although we cannot exclude that Bace1 and APP might reside on rafts for very short times (the temporal resolution of our tracking settings might not be not sufficiently high), we can at least conclude that APP and Bace1 do not undergo long range diffusion as part of stable membrane microdomains, and that Bace1 can move and reach APP, rather than the opposite.

Increased levels of cholesterol were expected to make the plasma membrane more compact, promoting the formation of rafts and the translocation of APP with subsequent reduction in mobility.[42] Nevertheless, the diffusion of APP was significantly lower only at 0.2 mg/mL β-CD-chol (curiously the same concentration at which also the levels of intracellular mBFP-sAPPβ were significantly increased), whereas at 0.4, 0.8 and 1.0 mg/mL β-CD-chol the mobility was higher compared to basal conditions. With the exception of 0.8 mg/mL β-CD-chol, the lateral diffusion of Bace1 did not seem particularly influenced by cholesterol. Although cholesterol can moderately change the mobility of APP on the plasma membrane, our results do not provide any evidence to support the hypothesis that cholesterol can influence APP processing through a mechanism involving the re-localization of APP in rafts, in agreement with the idea that partitioning of APP and Bace1 into rafts alone would not to be sufficient to induce β-secretase cleavage.[21] Our results align with previous studies on the effect of cholesterol loading on the mobility of membrane proteins in living cells, substantially different from the results obtained in liposomes, showing similar effects on the diffusion of some raft and non-raft proteins,[24] and more or less significant effects on mobility, sometimes with opposite results.[46] As the plasma membrane is the most raft-enriched membrane compartment in the cell, in which proteins with high raft affinity tend to localize,[47] it seems unlikely that a different dynamic behavior would occur on the endosome membrane. Our current technology did not however allow us to test this hypothesis.

Our data support the idea that changes in APP processing by Bace1 driven by cholesterol enrichment are not strongly dependent on variations in lateral diffusion that could change the substrate/enzyme proximity on the plasma membrane.[13]

Limitations of the study

Flow cytometry

With our approach we cannot discriminate if cholesterol affects only the processing, or the intracellular distribution of APP and subsequently the processing.

Western blots

The changes observed in western blots in shedding rate are within 10%, hardly appreciable by eye. Although we used an ECL substrate kit which has mid-femtogram levels of sensitivity, we had to repeat several times (at least 6) western blots experiments to find statistical significance. With this respect, flow cytometry analyses the fluorescence of several thousands of individual cells for each experiment, has a very high sensitivity and a lower number of variables that can influence the results, contributing to obtain results in a framework with a much higher statistical power than western blotting.

It is very difficult to find a proper loading control for the extracellular medium. The signal from serum proteins such as albumin will be too high and would not properly work as loading control for normalization (it would not change in a manner proportional to the number of grown cells). The possibility to use very

specific antibodies to measure the ratio between sAPPβ and sAPPα represents a reliable alternative, although it does not allow discriminating if it is sAPPβ that increases, or sAPPα that decreases.

Single molecule tracking

It is technically not possible to run single molecule tracking experiments in endosomes. We believe nevertheless that the plasma membrane is more similar to the endosomal membrane than artificial liposomes, and that our experiments can provide alternative useful data in relation to the hypothesis present in literature on the effect of cholesterol on raft localization of APP and Bace1.

STAR★METHODS

Detailed methods are provided in the online version of this paper and include the following:

- KEY RESOURCES TABLE
- RESOURCE AVAILABILITY
  - Lead contact
  - Materials availability
  - Data and code availability
- EXPERIMENTAL MODEL AND SUBJECT DETAILS
- METHOD DETAILS
  - Cloning
  - Cell transfection
  - Surface labeling
  - Modulation and evaluation of membrane cholesterol content
  - MTT reduction assay
  - Caspase-3 assay
  - Lipid peroxidation
  - FACS flow cytometry
  - Western blotting
  - Single molecule imaging and tracking
- QUANTIFICATION AND STATISTICAL ANALYSIS
  - Quantitative analysis of the diffusion coefficient
  - Statistical analysis

SUPPLEMENTAL INFORMATION

Supplemental information can be found online at https://doi.org/10.1016/j.isci.2023.106611.

AUTHOR CONTRIBUTIONS

Designed research: M.C. Performed research: C.Ca., A.B., N.P., M.E., N.B., R.C., L.M., M.C. Contributed analytic tools: M.C., C.Ce., F.S.P., F.A. Analyzed data: C.Ca., A.B., R.C., M.C. Wrote the paper: C.Ca, L.M., C.Ce., M.C.

DECLARATION OF INTERESTS

The authors declare no competing interests.

INCLUSION AND DIVERSITY

We support inclusive, diverse, and equitable conduct of research.

REFERENCES

1. Tiwari, S., Atluri, V., Kaushik, A., Yndart, A., and Nair, M. (2019). Alzheimer's disease: pathogenesis, diagnostics, and therapeutics. IJN 14, 5541–5554. https://doi.org/10.2147/IJN.S200490.

2. Wilquet, V., and De Strooper, B. (2004). Amyloid-beta precursor protein processing in neurodegeneration. Curr. Opin. Neurobiol. 14, 582–588. https://doi.org/10.1016/j.conb.2004.08.001.

3. O'Brien, R.J., and Wong, P.C. (2011). Amyloid precursor protein processing and Alzheimer's disease. Annu. Rev. Neurosci. 34, 185–204. https://doi.org/10.1146/annurev-neuro-061010-113613.

4. Zhang, H., Ma, Q., Zhang, Y.-W., and Xu, H. (2012). Proteolytic processing of Alzheimer's β-amyloid precursor protein. J. Neurochem. 120, 9–21. https://doi.org/10.1111/j.1471-4159.2011.07519.x.

5. Shepardson, N.E., Shankar, G.M., and Selkoe, D.J. (2011). Cholesterol level and statin use in Alzheimer disease: I. Review of epidemiological and preclinical studies. Arch. Neurol. 68, 1239–1244. https://doi.org/10.1001/archneurol.2011.203.

6. Fonseca, A.C.R., Resende, R., Oliveira, C.R., and Pereira, C.M.F. (2010). Cholesterol and statins in Alzheimer's disease: current controversies. Exp. Neurol. 223, 282–293. https://doi.org/10.1016/j.expneurol.2009.09.013.

7. Allinquant, B., Clamagirand, C., and Potier, M.-C. (2014). Role of cholesterol metabolism in the pathogenesis of Alzheimer's disease. Curr. Opin. Clin. Nutr. Metab. Care 17, 319–323. https://doi.org/10.1097/MCO.0000000000000069.

8. Ledesma, M.D., and Dotti, C.G. (2012). Peripheral cholesterol metabolic disorders and Alzheimer s disease. Front. Biosci. 4, 181–194. https://doi.org/10.2741/e368.

9. Koutsodendris, N., Nelson, M.R., Rao, A., and Huang, Y. (2022). Apolipoprotein E and Alzheimer's disease: findings, hypotheses, and potential mechanisms. Annu. Rev. Pathol. 17, 73–99. https://doi.org/10.1146/annurev-pathmechdis-030421-112756.

10. Sun, J.-H., Yu, J.-T., and Tan, L. (2015). The role of cholesterol metabolism in Alzheimer's disease. Mol. Neurobiol. 51, 947–965. https://doi.org/10.1007/s12035-014-8749-y.

11. Wang, C., Shou, Y., Pan, J., Du, Y., Liu, C., and Wang, H. (2019). The relationship between cholesterol level and Alzheimer's disease-associated APP proteolysis/Aβ metabolism. Nutr. Neurosci. 22, 453–463. https://doi.org/10.1080/1028415X.2017.1416942.

12. Abad-Rodriguez, J., Ledesma, M.D., Craessaerts, K., Perga, S., Medina, M., Delacourte, A., Dingwall, C., De Strooper, B., and Dotti, C.G. (2004). Neuronal membrane cholesterol loss enhances amyloid peptide generation. J. Cell Biol. 167, 953–960. https://doi.org/10.1083/jcb.200404149.

13. von Arnim, C.A.F., von Einem, B., Schneckenburger, H., Weber, P., Wagner, M., Schwanzar, D., Spoelgen, R., Strauss, W.L.S., and Schneckenburger, H. (2008). Impact of cholesterol level upon APP and BACE proximity and APP cleavage. Biochem. Biophys. Res. Commun. 370, 207–212. https://doi.org/10.1016/j.bbrc.2008.03.047.

14. Ye, S., Huang, Y., Müllendorff, K., Dong, L., Giedt, G., Meng, E.C., Cohen, F.E., Kuntz, I.D., Weisgraber, K.H., and Mahley, R.W. (2005). Apolipoprotein (apo) E4 enhances amyloid β peptide production in cultured neuronal cells: ApoE structure as a potential therapeutic target. Proc. Natl. Acad. Sci. USA 102, 18700–18705. https://doi.org/10.1073/pnas.0508693102.

15. Kalvodova, L., Kahya, N., Schwille, P., Ehehalt, R., Verkade, P., Drechsel, D., and Simons, K. (2005). Lipids as modulators of proteolytic activity of BACE. J. Biol. Chem. 280, 36815–36823. https://doi.org/10.1074/jbc.M504484200.

16. Marquer, C., Devauges, V., Cossec, J.-C., Liot, G., Lécart, S., Saudou, F., Duyckaerts, C., Lévêque-Fort, S., and Potier, M.C. (2011). Local cholesterol increase triggers amyloid precursor protein-Bace1 clustering in lipid rafts and rapid endocytosis. FASEB J. 25, 1295–1305. https://doi.org/10.1096/fj.10-168633.

17. Ghribi, O., Larsen, B., Schrag, M., and Herman, M.M. (2006). High cholesterol content in neurons increases BACE, beta-amyloid, and phosphorylated tau levels in rabbit hippocampus. Exp. Neurol. 200, 460–467. https://doi.org/10.1016/j.expneurol.2006.03.019.

18. Cossec, J.-C., Simon, A., Marquer, C., Moldrich, R.X., Leterrier, C., Rossier, J., Duyckaerts, C., Lenkei, Z., and Potier, M.-C. (2010). Clathrin-dependent APP endocytosis and Aβ secretion are highly sensitive to the level of plasma membrane cholesterol. Biochim. Biophys. Acta 1801, 846–852. https://doi.org/10.1016/j.bbalip.2010.05.010.

19. von Einem, B., Weber, P., Wagner, M., Malnar, M., Kosicek, M., Hecimovic, S., Arnim, C.A.F.v., and Schneckenburger, H. (2012). Cholesterol-dependent Energy transfer between fluorescent proteins—insights into protein proximity of APP and BACE1 in different membranes in niemann-pick type C disease cells. Indian J. Manag. Sci. 13, 15801–15812. https://doi.org/10.3390/ijms131215801.

20. Sonnino, S., Aureli, M., Grassi, S., Mauri, L., Prioni, S., and Prinetti, A. (2014). Lipid rafts in neurodegeneration and neuroprotection. Mol. Neurobiol. 50, 130–148. https://doi.org/10.1007/s12035-013-8614-4.

21. Ehehalt, R., Keller, P., Haass, C., Thiele, C., and Simons, K. (2003). Amyloidogenic processing of the Alzheimer β-amyloid precursor protein depends on lipid rafts. J. Cell Biol. 160, 113–123. https://doi.org/10.1083/jcb.200207113.

22. Brown, D.A. (2015). Preparation of detergent-resistant membranes (DRMs) from cultured mammalian cells. In Methods in Membrane Lipids Methods in Molecular Biology, D.M. Owen, ed. (Springer), pp. 55–64. https://doi.org/10.1007/978-1-4939-1752-5_5.

23. Kusumi, A., Fujiwara, T.K., Tsunoyama, T.A., Kasai, R.S., Liu, A.-A., Hirosawa, K.M., Kinoshita, M., Matsumori, N., Komura, N., Ando, H., and Suzuki, K.G.N. (2020). Defining raft domains in the plasma membrane. Traffic 21, 106–137. https://doi.org/10.1111/tra.12718.

24. Kenworthy, A.K., Nichols, B.J., Remmert, C.L., Hendrix, G.M., Kumar, M., Zimmerberg, J., and Lippincott-Schwartz, J. (2004). Dynamics of putative raft-associated proteins at the cell surface. J. Cell Biol. 165, 735–746. https://doi.org/10.1083/jcb.200312170.

25. Mundhara, N., Majumder, A., and Panda, D. (2019). Methyl-β-cyclodextrin, an actin depolymerizer augments the antiproliferative potential of microtubule-targeting agents. Sci. Rep. 9, 7638. https://doi.org/10.1038/s41598-019-43947-4.

26. Lambert, D., O'Neill, C., and Padfield, P.J. (2007). Methyl-β-Cyclodextrin increases permeability of caco-2 cell monolayers by displacing specific claudins from cholesterol rich domains associated with tight junctions. Chem. Pharm. Bull. 20, 495–506. https://doi.org/10.1159/000107533.

27. Sirtori, C.R. (2014). The pharmacology of statins. Pharmacol. Res. 88, 3–11. https://doi.org/10.1016/j.phrs.2014.03.002.

28. Parenti, N., Del Grosso, A., Antoni, C., Cecchini, M., Corradetti, R., Pavone, F.S., and Calamai, M. (2017). Direct imaging of APP proteolysis in living cells. PeerJ 5, e3086. https://doi.org/10.7717/peerj.3086.

29. Nalivaeva, N.N., and Turner, A.J. (2013). The amyloid precursor protein: a biochemical enigma in brain development, function and disease. FEBS Lett. 587, 2046–2054. https://doi.org/10.1016/j.febslet.2013.05.010.

30. Calamai, M., and Pavone, F.S. (2018). Quantifying the proteolytic cleavage of plasma membrane proteins in living cells. Curr. Protoc. Cell Biol. 81, e58. https://doi.org/10.1002/cpcb.58.

31. Bera, S., Camblor-Perujo, S., Calleja Barca, E., Negrete-Hurtado, A., Racho, J., De Bruyckere, E., Wittich, C., Ellrich, N., Martins, S., Adjaye, J., and Kononenko, N.L. (2020). AP-2 reduces amyloidogenesis by promoting BACE1 trafficking and degradation in neurons. EMBO Rep. 21, e47954. https://doi.org/10.15252/embr.201947954.

32. Wong, L., Curtiss, L.K., Huang, J., Mann, C.J., Maldonado, B., and Roheim, P.S. (1992). Altered epitope expression of human interstitial fluid apolipoprotein A-I reduces its ability to activate lecithin cholesterol acyl transferase. J. Clin. Invest. 90, 2370–2375.

33. Drabikowski, W., Lagwińska, E., and Sarzala, M.G. (1973). Filipin as a fluorescent probe for the location of cholesterol in the membranes of fragmented sarcoplasmic reticulum. Biochim. Biophys. Acta 291, 61–70. https://doi.org/10.1016/0005-2736(73)90060-6.

34. Sisodia, S.S. (1992). Beta-amyloid precursor protein cleavage by a membrane-bound protease. Proc. Natl. Acad. Sci. USA 89, 6075–6079. https://doi.org/10.1073/pnas.89.13.6075.

35. Chen, Y.-T., Chen, W.-Y., Huang, X.-T., Xu, Y.-C., and Zhang, H.-Y. (2018). Iron dysregulates APP processing accompanying with sAPPα cellular retention and β-secretase inhibition in rat cortical neurons. Acta Pharmacol. Sin. 39, 177–183. https://doi.org/10.1038/aps.2017.113.

36. Shin, R.-W., Saido, T.C., Maeda, M., and Kitamoto, T. (2005). Novel α-secretase cleavage of Alzheimer's amyloid β precursor protein in the endoplasmic reticulum of COS7 cells. Neurosci. Lett. 376, 14–19. https://doi.org/10.1016/j.neulet.2004.11.032.

37. Klein, D.M., Felsenstein, K.M., and Brenneman, D.E. (2009). Cathepsins B and L differentially regulate amyloid precursor protein processing. J. Pharmacol. Exp. Therapeut. 328, 813–821. https://doi.org/10.1124/jpet.108.147082.

38. Henriques, A.G., Vieira, S.I., Crespo-López, M.E., Guiomar de Oliveira, M.A., da Cruz e Silva, E.F., and da Cruz e Silva, O.A.B. (2009). Intracellular sAPP retention in response to Aβ is mapped to cytoskeleton-associated structures. J. Neurosci. Res. 87, 1449–1461. https://doi.org/10.1002/jnr.21959.

39. Bodovitz, S., and Klein, W.L. (1996). Cholesterol modulates α-secretase cleavage of amyloid precursor protein (*). J. Biol. Chem. 271, 4436–4440. https://doi.org/10.1074/jbc.271.8.4436.

40. Bauereiss, A., Welzel, O., Jung, J., Grosse-Holz, S., Lelental, N., Lewczuk, P., Wenzel, E.M., Kornhuber, J., and Groemer, T.W. (2015). Surface trafficking of APP and BACE in live cells. Traffic 16, 655–675. https://doi.org/10.1111/tra.12270.

41. Kinoshita, A., Fukumoto, H., Shah, T., Whelan, C.M., Irizarry, M.C., and Hyman, B.T. (2003). Demonstration by FRET of BACE interaction with the amyloid precursor protein at the cell surface and in early endosomes. J. Cell Sci. 116, 3339–3346. https://doi.org/10.1242/jcs.00643.

42. Day, C.A., and Kenworthy, A.K. (2009). Tracking microdomain dynamics in cell membranes. Biochim. Biophys. Acta 1788, 245–253. https://doi.org/10.1016/j.bbamem.2008.10.024.

43. Vetrivel, K.S., and Thinakaran, G. (2010). Membrane rafts in Alzheimer's disease beta-amyloid production. Biochim. Biophys. Acta 1801, 860–867. https://doi.org/10.1016/j.bbalip.2010.03.007.

44. Karch, S., Broichhagen, J., Schneider, J., Böning, D., Hartmann, S., Schmid, B., Tripal, P., Palmisano, R., Alzheimer, C., Johnsson, K., and Huth, T. (2018). A new fluorogenic small-molecule labeling tool for surface diffusion analysis and advanced fluorescence imaging of β-site amyloid precursor protein-cleaving enzyme 1 based on silicone rhodamine: SiR-BACE1. J. Med. Chem. 61, 6121–6139. https://doi.org/10.1021/acs.jmedchem.8b00387.

45. Lenne, P.-F., Wawrezinieck, L., Conchonaud, F., Wurtz, O., Boned, A., Guo, X.-J., Rigneault, H., He, H.-T., and Marguet, D. (2006). Dynamic molecular confinement in the plasma membrane by microdomains and the cytoskeleton meshwork. EMBO J. 25, 3245–3256. https://doi.org/10.1038/sj.emboj.7601214.

46. Brameshuber, M., Weghuber, J., Ruprecht, V., Gombos, I., Horváth, I., Vigh, L., Eckerstorfer, P., Kiss, E., Stockinger, H., and Schütz, G.J. (2010). Imaging of mobile long-lived nanoplatforms in the live cell plasma membrane. J. Biol. Chem. 285, 41765–41771. https://doi.org/10.1074/jbc.M110.182121.

47. Kenworthy, A.K. (2020). Choosing who can ride the raft. Nat. Rev. Mol. Cell Biol. 21, 566–567. https://doi.org/10.1038/s41580-020-00285-y.

48. Howarth, M., Takao, K., Hayashi, Y., and Ting, A.Y. (2005). Targeting quantum dots to surface proteins in living cells with biotin ligase. Proc. Natl. Acad. Sci. USA 102, 7583–7588. https://doi.org/10.1073/pnas.0503125102.

49. Subach, O.M., Gundorov, I.S., Yoshimura, M., Subach, F.V., Zhang, J., Grüenwald, D., Souslova, E.A., Chudakov, D.M., and Verkhusha, V.V. (2008). Conversion of red fluorescent protein into a bright blue probe. Chem. Biol. 15, 1116–1124. https://doi.org/10.1016/j.chembiol.2008.08.006.

50. Pensalfini, A., Zampagni, M., Liguri, G., Becatti, M., Evangelisti, E., Fiorillo, C., Bagnoli, S., Cellini, E., Nacmias, B., Sorbi, S., and Cecchi, C. (2011). Membrane cholesterol enrichment prevents Aβ-induced oxidative stress in Alzheimer's fibroblasts. Neurobiol. Aging 32, 210–222. https://doi.org/10.1016/j.neurobiolaging.2009.02.010.

51. Bigi, A., Ermini, E., Chen, S.W., Cascella, R., and Cecchi, C. (2021). Exploring the release of toxic oligomers from α-synuclein fibrils with antibodies and STED microscopy. Life 11, 431. https://doi.org/10.3390/life11050431.

52. Gardini, L., Calamai, M., Hatakeyama, H., Kanzaki, M., Capitanio, M., and Pavone, F.S. (2018). Three-dimensional tracking of quantum dot-conjugated molecules in living cells. In Nanoscale Imaging Methods in Molecular Biology, Y.L. Lyubchenko, ed. (Springer New York), pp. 425–448. https://doi.org/10.1007/978-1-4939-8591-3_26.

53. Calamai, M., and Pavone, F.S. (2011). Single molecule tracking analysis reveals that the surface mobility of amyloid oligomers is driven by their conformational structure. J. Am. Chem. Soc. 133, 12001–12008. https://doi.org/10.1021/ja200951f.

54. Scotti, E., Calamai, M., Goulbourne, C.N., Zhang, L., Hong, C., Lin, R.R., Choi, J., Pilch, P.F., Fong, L.G., Zou, P., et al. (2013). IDOL stimulates clathrin-independent endocytosis and multivesicular body-mediated lysosomal degradation of the low-density lipoprotein receptor. Mol. Cell Biol. 33, 1503–1514. https://doi.org/10.1128/MCB.01716-12.

55. Calamai, M., and Pavone, F.S. (2013). Partitioning and confinement of GM1 ganglioside induced by amyloid aggregates. FEBS Lett. 587, 1385–1391. https://doi.org/10.1016/j.febslet.2013.03.014.

56. Bannai, H., Lévi, S., Schweizer, C., Dahan, M., and Triller, A. (2006). Imaging the lateral diffusion of membrane molecules with quantum dots. Nat. Protoc. 1, 2628–2634. https://doi.org/10.1038/nprot.2006.429.

57. Ehrensperger, M.-V., Hanus, C., Vannier, C., Triller, A., and Dahan, M. (2007). Multiple association states between glycine receptors and gephyrin identified by SPT analysis. Biophys. J. 92, 3706–3718. https://doi.org/10.1529/biophysj.106.095596.

58. Tinevez, J.-Y., Perry, N., Schindelin, J., Hoopes, G.M., Reynolds, G.D., Laplantine, E., Bednarek, S.Y., Shorte, S.L., and Eliceiri, K.W. (2017). TrackMate: an open and extensible platform for single-particle tracking. Methods 115, 80–90. https://doi.org/10.1016/j.ymeth.2016.09.016.

59. Saxton, M.J., and Jacobson, K. (1997). Single-particle tracking: applications to membrane dynamics. Annu. Rev. Biophys. Biomol. Struct. 26, 373–399. https://doi.org/10.1146/annurev.biophys.26.1.373.

60. Kusumi, A., Sako, Y., and Yamamoto, M. (1993). Confined lateral diffusion of membrane receptors as studied by single particle tracking (nanovid microscopy). Effects of calcium-induced differentiation in cultured epithelial cells. Biophys. J. 65, 2021–2040.

61. Triller, A., and Choquet, D. (2008). New concepts in synaptic biology derived from single-molecule imaging. Neuron 59, 359–374. https://doi.org/10.1016/j.neuron.2008.06.022.

STAR★METHODS

KEY RESOURCES TABLE

REAGENT or RESOURCE	SOURCE	IDENTIFIER
Antibodies		
Rabbit anti-HA antibody	Abcam	Cat#ab9110; RRID:AB_307019
Secondary goat anti-rabbit Alexa Fluor 568 antibody	Abcam	Cat#ab175471; RRID:AB_2576207
Anti-Human sAPPβ-WildType	IBL	Cat#18957; RRID:AB_2302034
Anti-Human sAPPα	IBL	Cat#11088; RRID:AB_494690
Anti-Human APP (C)	IBL	Cat#18961; RRID:AB_2056701
Anti-alpha Tubulin antibody	Abcam	Cat#ab7291; RRID:AB_2241126
Anti-rabbit Fab-QDs 655	Invitrogen	Cat#Q11422MP; RRID:AB_10375438
Anti-rabbit Fab-QDs 585	Invitrogen	Cat#Q-11411MP; RRID:AB_2556470
Chemicals, peptides, and recombinant proteins		
Protease Inhibitor Cocktail powder	Sigma-Aldrich	Cat#P2714-1BTL
Paraformaldehyde	Sigma-Aldrich	Cat#8.18715
Sodium dodecyl sulfate	Sigma-Aldrich	Cat#436143
N, N-dimethylformamide	Sigma-Aldrich	Cat#319937
Filipin III	Sigma-Aldrich	Cat#F4767
FAM-FLICA Caspase-3/7 solution	Immunochemistry Technologies	Cat#93
BODIPY 581/591C11	Thermo Fisher Scientific	Cat#D3861
Dimethyl sulfoxide	Sigma-Aldrich	Cat#D8418
BirA	Howarth et al.[48]	N/A
streptavidin-QDs 655	Invitrogen	Cat#Q10123MP
Critical commercial assays		
Fluorimetric Amplex Red Cholesterol Assay Kit	Thermo Fisher Scientific	Cat#A12216
Bradford Protein Assay	Bio-Rad	Cat#5000201
PierceTM Rapid Gold BCA (bicinchoninic acid) Protein Assay	Thermo Fisher Scientific	Cat# A53226
Experimental models: Cell lines		
Human SH-SY5Y neuroblastoma cells	ATCC	Cat#CRL-2266
Oligonucleotides		
Primers for Nhel and Ascl restriction sites insertion: Forward: TAAGCAGCTAGCA TGAGCGAGCTGATTAAGG; Reverse: TGGCGCGCCTGTTCCACGACTATTA AGCTTGTGCCCCAG	This paper	N/A
Primers for HA sequence insertion: Forward: CTAGCTATCCGTACGACGTACCAGACTA CGCAGG; Reverse: CGCGCCTGCGTAGTC TGGTACGTCGTACGGATAG)	This paper	N/A
Recombinant DNA		
Construct: mBFP-APP-mGFP	Addgene	196694
Construct: mBFP-APPP1-mGFP	Addgene	196695

Continued

REAGENT or RESOURCE	SOURCE	IDENTIFIER
Construct: HA-APP-mGFP	Addgene	196696
Construct: HA-BACE1-mBFP	Addgene	196697
Construct: mCherry-APP-mGFP	Addgene	196704
Construct: mCherry-APPP1-mGFP	Addgene	196705
Construct: AP-APP	Addgene	196706
Software and algorithms		
ImageJ	National Institutes of Health	https://imagej.nih.gov/ij/
MATLAB	MathWorks	

RESOURCE AVAILABILITY

Lead contact

Further information and requests for resources and reagents should be directed to and will be fulfilled by the lead contact, Martino Calamai (calamai@lens.unifi.it).

Materials availability

Plasmids generated in this study have been deposited to Addgene:

mBFP-APP-mGFP - ID 196694.

mBFP-APP^{P1}-mGFP - ID 196695.

HA-APP-mGFP - ID 196696.

HA-BACE1-mBFP - ID 196697.

mCherry-APP-mGFP - ID 196704.

mCherry-APP^{P1}-mGFP - ID 196705.

AP-APP - ID 196706.

Data and code availability

- All data reported in this paper will be shared by the lead contact upon request.
- This paper does not report original code.
- Any additional information required to reanalyze the data reported in this paper is available from the lead contact upon request.

EXPERIMENTAL MODEL AND SUBJECT DETAILS

Human SH-SY5Y neuroblastoma cells (A.T.C.C., USA, RRID:CVCL_0019) were cultured in Dulbecco's Modified Eagle's Medium (DMEM) (ThermoFisher Scientific, USA) F-12 Ham (1:1) supplemented with 10% Fetal Bovine Serum (FBS), 1.0 mM glutamine and 1% penicillin/streptomycin solution in a 5% CO_2 humidified atmosphere at 37°C and grown until 80% confluence for a maximum of 20 passages.

METHOD DETAILS

Cloning

To generate the fusion construct mBFP-APP-mGFP, we used the plasmid pCMV6-AN-mGFP already containing the sequence NheI-AscI-APP-mGFP.[28] The mBFP sequence was amplified from the plasmid pmTagBFP2-N1[49] by PCR, in order to insert the restriction sites for the NheI and AscI enzymes at the N- and C-terminal, respectively (forward primer: TAAGCAGCTAGCATGAGCGAGCTGATTAAGG, reverse primer: TGGCGCGCCTGTTCCACGACTATTAAGCTTGTGCCCCAG). After digestion, the sequence of

mBFP was inserted at the N-terminal of APP. The targeting of the fusion protein to the plasma membrane was ensured by the presence of a signal peptide (SP) located at the N-terminal immediately before the mBFP.

The fusion construct mBFP-APP[P1]-mGFP, which carries the mutation Lys612Val at position P1 in the APP gene, was generated in a similar way after removal of mCherry from mCherry-APP[P1]-mGFP[28] by digestion with NheI and AscI enzymes.

The plasmid pCMV6-AN-mGFP with the sequence NheI-AscI-APP-mGFP was also used to produce the fusion construct HA-APP-mGFP.[28] After digestion with the enzymes NheI and AscI, the annealed oligonucleotides containing the sequence for the HA tag (forward primer: CTAGCTATCCGTACGACGTACCAG ACTACGCAGG, reverse primer: CGCGCCTGCGTAGTCTGGTACGTCGTACGGATAG) were inserted in the plasmid.

The fusion constructs HA-BACE1-mBFP and AP-APP were obtained previously.[28]

Cell transfection

For the transfection, cells were plated in 12-well plates with or without coverslips (for imaging and flow cytometry experiments, respectively). 24 h after plating, the cells were transfected using Lipofectamine 2000 (Life Technologies), according to the manufacturer's instructions, with 1 μg DNA and 2 μL Lipofectamine in OPTIMEM medium.

Surface labeling

After two days of transfection with the chimeric constructs HA-APP-mGFP and HA-Bace1-mBFP, cells were washed with phosphate buffered saline (PBS, 0.5 mM $MgCl_2$, 0.8 mM $CaCl_2$, pH 7.4) and fixed in 4% (w/v) buffered paraformaldehyde (PFA) for 12 min at room temperature. Then, cells were blocked with a 30 min incubation with 4% bovine serum albumin (BSA) and incubated for 30 min with 1:500 diluted primary rabbit anti-HA antibody (ab9110 Abcam, UK). After incubation, cells were carefully washed and incubated for 30 min with 1:500 diluted secondary goat anti-rabbit Alexa Fluor 568 antibody (Abcam, UK). Coverslips were washed with PBS and water and mounted on a glass slide. Cell imaging was performed on a Nikon Eclipse TE300C2 confocal laser scanning (CLSM) (Nikon, Japan) equipped with a Nikon 60x immersion oil objective (Apo Plan, NA 1.4) and with Coherent CUBE (diode 405 nm), Melles Griot (Argon 488 nm) and Coherent Sapphire (Sapphire 561 nm) lasers. Emission filters for imaging were 452/45 nm (for mBFP), 514/30 nm (for mGFP) and 595/60 nm (for Alexa 568). Settings were maintained constant for each analysis. > 10 cells were analyzed for each examined sample by using ImageJ software (National Institutes of Health, Bethesda, MD, USA).

Modulation and evaluation of membrane cholesterol content

Membrane cholesterol content was increased by adding cholesterol conjugated to methyl-β-cyclodextrin (Sigma Adrich) to the cell culture medium of SH-SY5Y at different concentrations (0, 0.2, 0.4, 0.6, 0.8, and 1.0 mg/mL) for 3 h at 37°C. The cholesterol content in cellular membrane fractions was then assessed using the sensitive fluorimetric Amplex Red Cholesterol Assay Kit (Thermo Fisher Scientific) as reported previously,[50] according to the manufacturer's instructions. Membrane fractions were obtained as previously described, with minor modifications. Briefly, cells were dissolved in PBS containing 9% sucrose and a protease inhibitors cocktail (Sigma-Aldrich) 1:200 and then homogenized with three freeze–thaw cycles and three cycles of 30 s sonication on ice with intervals for cooling. The samples were centrifuged at 750×g for 10 min at 4°C and a further centrifugation of the supernatant was performed at 110,000×g for 1 h at 4°C to pellet the membrane fractions. The resulting pellets were re-suspended in PBS with 9% sucrose and the protease inhibitor cocktail 1:200 and protein concentrations were then determined by the Bradford Protein Assay (Bio-Rad, Hercules, CA, USA).

The distribution of membrane cholesterol was also investigated using the fluorescent probe filipin (Sigma-Aldrich) as previously described[50], with minor modifications. Briefly, SH-SY5Y cells seeded on glass coverslips were fixed in 4.0% buffered paraformaldehyde for 20 min and then incubated with 0.1 mg/mL filipin for 1 h at 37°C. After washing with PBS, the cells were fixed again in 4.0% buffered paraformaldehyde for 20 min at 0°C. The emitted fluorescence was detected after excitation at 355 nm using a confocal Leica TCS SP8 scanning confocal microscopy system (Leica Microsystems, Mannheim, Germany) equipped with an argon

laser source. A series of 1.0 μm thick optical sections (1024 × 1024 pixels) was taken through the cell depth for each sample using a Leica Plan Apo 63× oil immersion objective and projected as a single composite image by superimposition. The confocal microscope was set at optimal acquisition conditions, e.g., pinhole diameters, detector gain and laser powers. Settings were maintained constant for each analysis.

MTT reduction assay

The mitochondrial functionality of SH-SY5Y cells seeded in 96-well plates was assessed upon cholesterol enrichment by the 3-(4,5-dimethylthiazol-2-yl)-2,5-diphenyltetrazolium bromide (MTT) assay, as previously described.[51] Briefly, after 3h of enrichment, cells were incubated with the MTT solution for 4 h. Then, a cell lysis buffer (20% sodium dodecyl sulfate (SDS), 50% N, N-dimethylformamide, pH 4.7) was added for 1 h to solubilize the formazan product. The absorbance values of blue formazan were measured at 590 nm using the Microplate Manager Software (Biorad, CA, USA). Cell viability was expressed as the percentage of MTT reduction in enriched cells with respect to basal ones.

Caspase-3 assay

The levels of caspase-3 activity were analyzed after membrane cholesterol enrichment of SH-SY5Y cells seeded on glass coverslips, by using the FAM-FLICA Caspase-3/7 assay kit (Immunochemistry Technologies, LLC, Bloomington, MN) containing the FAM-DEVD-FMK reagent that binds to active caspase-3, and by the confocal scanning system as previously reported.[51] Treatment with 250 μM H_2O_2 for 3 h was applied as a positive control for caspase-3 activation.

Lipid peroxidation

Membrane lipid peroxidation was investigated by confocal microscope analysis of the green (ex 485 nm/em 520 nm) and red signal (ex 581 nm/em 591 nm) of the fluorescent probe BODIPY 581/591 C11 (Thermo Fisher Scientific), as previously reported.[50] In particular, BODIPY 581/591 C11 shifts its fluorescence from red to green when challenged with oxidizing agents. Briefly, after membrane cholesterol enrichment of SH-SY5Y cells seeded on glass coverslips, the fluorescent probe BODIPY dissolved in 0.1% DMSO was added to the cell culture media (5.0 μM final concentration) for 30 min at 37°C. The cells were fixed in 2.0% buffered paraformaldehyde for 10 min at room temperature and the BODIPY fluorescence was analyzed by the confocal scanning system previously described, using 581 nm excitation wavelength. Treatment with 250 μM H_2O_2 for 3h was applied as a positive control for membrane lipid peroxidation.

FACS flow cytometry

Cells were harvested after mild trypsin treatment and were washed and re-suspended in PBS and FBS 1% to inhibit trypsin activity. Flow cytometry was performed by using a BD LSRII flow cytometer ((BDBioscience, Becton Dickinson, USA)) equipped with 405 and 488 nm lasers. mBFP was excited with the 405 nm laser and its fluorescence was collected through a 440/40 nm band-pass filter band-pass filter. mGFP was excited using the 488 nm laser, and the emitted fluorescence was collected through a 530/30 nm band-pass filter. In case of the construct mCherry-APP-mGFP, flow cytometry was performed by using an S3 flow cytometer (Bio-Rad) equipped with 488 and 561 nm diode-pumped solid-state lasers. mGFP was excited using the 488 nm laser, and the emitted fluorescence was collected through a 525/30 nm band-pass filter; mCherry was excited with the 561 nm laser and its fluorescence was collected through a 615/25 nm band-pass filter.

Data were analyzed using the free Flowing software (Cell Imaging and Cytometry Core, Turku Bioscience Center, Finland). The cellular debris was excluded from the quantification by gating cells on the Forward scatter area/Side scatter area (FSC/SSC). Approximately 10000 events were acquired for each sample.

Western blotting

Human SH-SY5Y neuroblastoma cells stably transfected with mBFP-APP-mGFP were cultured in 12 wells plates. 3 h after incubation with different concentrations of β-CD-chol, the extracellular medium was recovered and the cells were lysed using 300 μL of PBS and Laemmli buffer. Lysed cells were collected in safe lock 1.5 mL tubes and immersed in boiling water for 5 min, then sonicated two times for 15 s and boiled again for 5 min. The recovered medium was centrifuged at 10000 rpm for 5 min in order to remove cell debris and other impurity, and then treated as the cell lysate. Total protein levels were quantified using the Pierce Rapid Gold BCA (bicinchoninic acid) Protein Assay (ThermoFisher Scientific, USA). Extracellular medium

and lysate samples were loaded in pre-casted polyacrylamide gels (ThermoFisher Scientific, USA) and blotted on PVDF membranes (ThermoFisher Sicnetific, USA). Membranes were blocked in 5% milk in PBST overnight at 4°C or 1 hat room temperature. After blocking, membranes were rinsed three times with PBST and incubated overnight at 4°C with primary antibody (in PBST with 4% BSA) and for an additional hour at room temperature with secondary anti-rabbit antibody conjugated to horseradish peroxidase. The primary antibodies were: Anti-Human sAPPβ-WildType (IBL 18957), Anti-Human sAPPα (IBL 11088), Anti-Human APP (C) (IBL 18961) and Anti-alpha Tubulin antibody (Abcam ab7291) at the concentrations indicated by the manufacturer. Membranes were rinsed with the HRP substrate Pico Dura (ThermoFisher Scientific, USA) and imaged after 5 min with a Chemidoc MP system (Bio-Rad, USA). In order to perform the stripping procedure, the blotted PVDF membranes were covered with Seppro Stripping Buffer (Sigma Aldrich, USA) and incubated for 5–10 minat room temperature. The stripping buffer was then discarded and the incubation was repeated with fresh Seppro buffer for 5–10 min. After discarding the buffer, membranes were washed for two times with PBS for 10 min, then washed for two times with TBST for 5 min and blocked.

Single molecule imaging and tracking

The methods that we used for quantum dot (QD) labeling and live imaging have been already reported.[52–55] Living cells transfected for 48 h with HA-APP-mGFP and HA-BACE1-mBFP plasmids were incubated in phenol red-free Leibovitz's L-15 medium 3% FBS at 37°C with anti-HA primary antibody (1:150,000) for 5 min, then for 5 min with anti-rabbit Fab-QDs 655 (Invitrogen, 1:1000). For dual color single molecule tracking, AP-APP was co-transected with HA-BACE1-mBFP and BirA, a biotin ligase that specifically biotinylates the AP tag.[48] Biotin was added to the cell medium (final concentration 10 μM) 8 h after transfection and 12 h before imaging. Cells were then incubated as above with streptavidin-QDs 655 (Invitrogen, 1:10,000) and anti-rabbit Fab-QDs 585 (Invitrogen, 1:1000) in QD binding buffer for 1 min. The cells were monitored with an Olympus IX2-UCB wide-field epifluorescence microscope equipped with a 100x UPlanSAPO Olympus oil-immersion objective, a four-channel LED Driver Thorlabs DC4014 (using 405 excitation LED) and a custom heating chamber set at 37°C. Dichoric FF552-Di02 and emission FF02-655/40-25 filters were used for QDs emitting at 655 nm. For dual color tracking experiments, a first dichroic FF552-Di02 filter was followed by an Hamamatsu W-view Gemini dual viewer equipped with an FF624 di01 and FF02-655/40-25 (for streptavidin-QDs 655) and FF01-585/40-25 (for Fab-QDs 585) emission filters. All filters were from Semrock. Movies were acquired with an integration time of 100 ms with an Electron Multiplying Charge-Coupled ImageMX2 camera (Hamamatsu).

Recording sessions did not last more than 30 min. Tracking of single QDs, identified by their fluorescence intermittence, was performed with MATLAB (MathWorks) using a homemade macro that accounts for blinking in the fluorescence signal.[56,57] In brief, the method consisted of two main steps, applied successively to each frame of the sequence. First, the fluorescent spots were detected by cross-correlating the image with a Gaussian model of the Point Spread Function. A least-squares Gaussian fit was applied (around the local maximum above a threshold) to determine the center of each spot with a spatial accuracy of 10–20 nm (depending on the signal-to-noise ratio). Second, QD trajectories were assembled automatically by linking, frame to frame, the centers of the fluorescent spots likely coming from the same QD. The association criterion was based on the assumption of free Brownian diffusion and took into account short blinking events. After completion of the process, a manual association step was performed, in which QD trajectories of maximal length were assembled from smaller fragments separated by longer blinking events that were not taken into account by the automatic linking procedure. The movies were realized with TrackMate.[58]

QUANTIFICATION AND STATISTICAL ANALYSIS

Quantitative analysis of the diffusion coefficient

The mean square displacement (MSD) analysis allows for calculating the initial diffusion coefficient (D) of each particle.[56,57] Briefly, physical parameters can be extracted from each trajectory (x(t),Bace(t)) by computing the MSD,[59] as calculated from the following formula:

$$MSD(ndt) = \frac{1}{N-n} \sum_{i=1}^{N-n} \left[\left(x_{(i+n)} - x_i\right)^2 + \left(y_{(i+n)} - y_i\right)^2 \right]$$

where x_i and y_i are the coordinates of a particle on frame i, dt is the time between two successive frames, N the total number of frames of the trajectory and ndt the time interval over which the displacement is averaged. This function enables the analysis of the lateral dynamics on short (initial diffusion coefficient) and long (types of motion) time scales. Different types of motion can be distinguished from the time dependence of the MSD.[59] The initial diffusion coefficient (D) is determined by fitting the initial 2 to 5 points of the MSD against time plot with MSD(t) = $4D_{2-5}$ t + b.

The size of the domain of confinement was estimated by fitting the convenient MSD with the expected generic expression for a confined diffusion[60,61]:

$$MSD(t) = \frac{L^2}{3}\left(1 - exp\left(-\frac{12Dt}{L^2}\right)\right)$$

where L is the side of a square domain in which diffusion is supposed to be restricted.

Trajectories movies and mean speed of QDs were obtained with Trackmate[58] plug-in of ImageJ.

Statistical analysis

The linear correlation coefficient r was used to assess the statistical significance of increased cholesterol concentrations on APP processing and diffusion of APP and Bace1. Student's $t$test or Kolmogorov-Smirnov's test were used to compare distributions as indicated in corresponding Figure legends. Error bars were expressed as mean $\pm$ Standard Deviation (S.D.), or mean $\pm$ Standard Errors of the Means (S.E.M.), as indicated in corresponding Figure legends. In the case of diffusion coefficient D, we compared cumulative probability distributions and median instead of mean values because D values were spread over 4 orders of magnitude. In general, a pvalue lower than 0.05 was considered statistically significant. The single (*), double (**) and triple (***) asterisks refer to pvalues lower than 0.05, 0.01 and 0.001. The statistical details of the experiments can be found in the Figures and corresponding legends. Statistical analysis was performed using KaleidaGraph or Graphpad software.